Chapter 6

Resonances in Left-Handed Waves Developed in Nonlinear Electrical Lattices

Koichi Narahara

Additional information is available at the end of the chapter

http://dx.doi.org/10.5772/intechopen.70739

Abstract

We investigate resonant interactions in a specific electrical lattice that supports left-handed (LH) waves. The impact of LH waves on the three-wave mixing process, which is the most fundamental resonant interaction, is illustrated. In contrast to the ordinary right-handed (RH) waves, the phase of the LH wave moves to the different direction from its power. This exotic property together with the lattice's dispersive features results in the resonant phenomena that are effectively utilized for practical electrical engineering, including the significant harmonic wave generation via head-on collisions, harmonic resonance, and short pulse generation driven by soliton decay. These resonances are quantified by the asymptotic expansion and characterized by numerical and/or experimental methods, together with several design criteria for their practical utilization. To cope with dissipation, a field-effect transistor (FET) is introduced in each cell. In particular, we characterize the stationary pulse resulting from the balance between dissipation and FET gain.

Keywords: three-wave mixing, soliton decay, harmonic resonance, left-handedness, electrical lattices, composite right- and left-handed transmission lines, traveling-wave field-effect transistors, coherent structures

1. Introduction

Resonances have been utilized as the powerful tool to achieve harmonic wave generation in electrical engineering. This chapter introduces left-handedness to the interacting waves and discusses its impact in that field. In ordinary, that is, right-handed (RH) media, the wave vector directs to the same direction as the Poynting vector, so that the phase and power move to a common direction. In left-handed (LH) media, the situation is reversed.

To achieve strong resonant interactions, frequencies and wave numbers must be preserved. For example, when a wave of frequency ω_1 and wave number k_1 interacts with one of ω_3 and k_3, a

significant third wave of ω_2 and k_2 will be generated if the conditions $\omega_1 + \omega_3 = \omega_2$ and $k_1 + k_3 = k_2$ are satisfied. The sum of the wavenumber decreases for the head-on collision, because the wave vector of the left-moving wave has the opposite sign as that of the right-moving one. In contrast, the sum frequency increases. The phase and power are transferred with the phase and group velocities, respectively. In addition, the group velocity is given by the slope of the dispersion curve, so that the frequency increases at least locally as the wavenumber decreases in LH media, so that they can satisfy the resonant conditions for head-on colliding waves.

To investigate resonances involving LH waves, we introduce nonlinearity to composite right- and left-handed (CRLH) transmission lines. CRLH transmission lines have been investigated in electrical engineering community as the practical and broadband platform to support LH waves [1–4]. The line has noteworthy dispersive property that the propagating wave exhibits LH (RH) properties when its carrier frequency is greater (less) than the line's characteristic frequencies. Furthermore, several activities have clarified the wave dynamics in CRLH lines with nonlinearity introduced by voltage-controlled devices [5–13]. In our case, the shunt capacitor each cell of a CRLH line contains is replaced with the Schottky varactor [10, 14]. The three-wave resonant interaction (3WRI) equations have been derived from the transmission equations of that nonlinear CRLH line via the derivative expansion method and is used to characterize the head-on collision of LH waves.

Even when $\omega_1 = \omega_3$ and $k_1 = k_3$, the significant energy is transferred from the fundamental to the second harmonic when the conditions $\omega_2 = 2\omega_1$ and $k_2 = 2k_1$ are satisfied. This process, termed harmonic resonance, is a special case of the three-wave resonant interaction, resulting from resonance of two identical waves. The dispersion of a nonlinear CRLH line can cause harmonic resonance for the LH fundamental and RH second harmonic waves. The phase of the LH fundamental wave advances toward the input end. Accordingly, that of the second harmonic wave should also move to the input. Because the fundamental wave increases to that direction, the harmonic resonance generates the second harmonic wave more when it travels longer. The generation efficiency of the second harmonic waves becomes enhanced through this behavior via supplemental cavity resonance. It should be noted that the fundamental wave is spontaneously converted into its second harmonic one without the aid of pump waves.

Similar spontaneous resonant interaction is expected in nonlinear CRLH lines. The soliton decay is realized for three waves having different group velocities. It requires the situation where the wave having the middle group velocity is incident to the line. Then, a soliton contained in the incident wave decays into the fast and slow solitons spontaneously. Inevitably, the slow soliton(s) occupies the LH branch for the nonlinear CRLH line; therefore, it starts to travel to the opposite direction to the incident and fast solitons, leading to the shortening of the fast soliton. By solving the eigenvalue problem of the Zakharov-Shabat (ZS) equation relating with the 3WRI equation, it is found that the fast soliton can become shorter for longer incident wave. Through these observations, we can utilize the soliton decay in the nonlinear CRLH line for generating broadband envelope pulses.

The use of nonlinear CRLH lines is sometimes limited because of wave attenuation caused by finite electrode resistance and substrate current leakage. In order to achieve loss compensation, a traveling-wave field-effect transistor (TWFET) is considered [15]. For the voltage waves

http://dx.doi.org/10.5772/intechopen.70739

traveling over FET electrodes, two CRLH lattices are required, which are, respectively, loaded with the gate and drain in each cell. The unit-cell FET can be biased via the LH inductors. In addition, the inter-cell direct current flow is cut off by the LH capacitors. The device introduces LC resonant pairs in each cell, which can operate as nonlinear oscillators with the aid of FET gain; therefore, the device can be considered as a kind of spatially extended oscillator systems. Hereafter, we call the device as the CRLH-TWFET. In the case of supercritical Andronov-Hopf bifurcation, the oscillation amplitude gradually increases when the bifurcation parameter passes a critical value. Then, the relaxation time needed to initiate autonomous oscillation becomes sufficiently large; therefore, it succeeds in effectively suppressing autonomous oscillation to guarantee the loss-compensated propagation of LH pulse waves. On the other hand, the amplitude grows to become discontinuously finite in subcritical cases, where the system affords the coexistence of an oscillatory region with a nonoscillatory region in addition to the homogeneous oscillatory state [16]. The resulting coherent structures function as the building blocks of the spatiotemporal patterns appearing in the system. When both boundaries at the ends of the oscillatory region preserve their relative positions, the oscillatory region preserving this envelope is called a pulse. Possibly, the boundary velocity vanishes, so that the pulse becomes localized and stationary [17, 18]. From the scientific viewpoint, a convenient electronic system to support such solitary waves is valuable for clarifying their interacting dynamics using either numerical or experimental method.

After describing the structure and dispersive properties of the nonlinear CRLH line, the head-on collision of envelope pulses is characterized numerically on that line to illustrate significant generation of harmonic waves through resonances. Next, the process is quantified by the 3WRI equations derived by applying the derivative expansion method to the transmission equations of a nonlinear CRLH line. Subsequently, two spontaneous resonant interactions: harmonic resonance and soliton decay are characterized, where the same 3WRI equations are used to model the wave dynamics. Finally, the development of a stationary pulse in a CRLH-TWFET is discussed.

2. Fundamental properties of nonlinear CRLH TLs

Because the nonlinear electrical lattice we investigate is based on CRLH lines, we first describe their fundamental properties. The unit-cell structure is shown at the top of **Figure 1(a)**, where C_R, L_R, C_L, and L_L represent the shunt capacitor, series inductor, series capacitor, and shunt inductor, respectively. It is shown that two different frequencies are allowed to be supported on the line for a wavenumber k. As shown below, the high frequency mode exhibits a RH property and the low frequency one becomes left-handed; therefore, we denote the dispersion relationships of the two as $\omega = \omega_{\mathrm{RH,LH}}(k)$ (ω_{RH} is for the RH and ω_{LH} for LH). Under the sixth order long wavelength approximation, these two are explicitly given by

$$\omega_{RH}(k) = \sqrt{\omega_x^2(k) + \sqrt{\omega_x^4(k) - \frac{1}{C_L C_0 L_L L_R}}}, \tag{1}$$

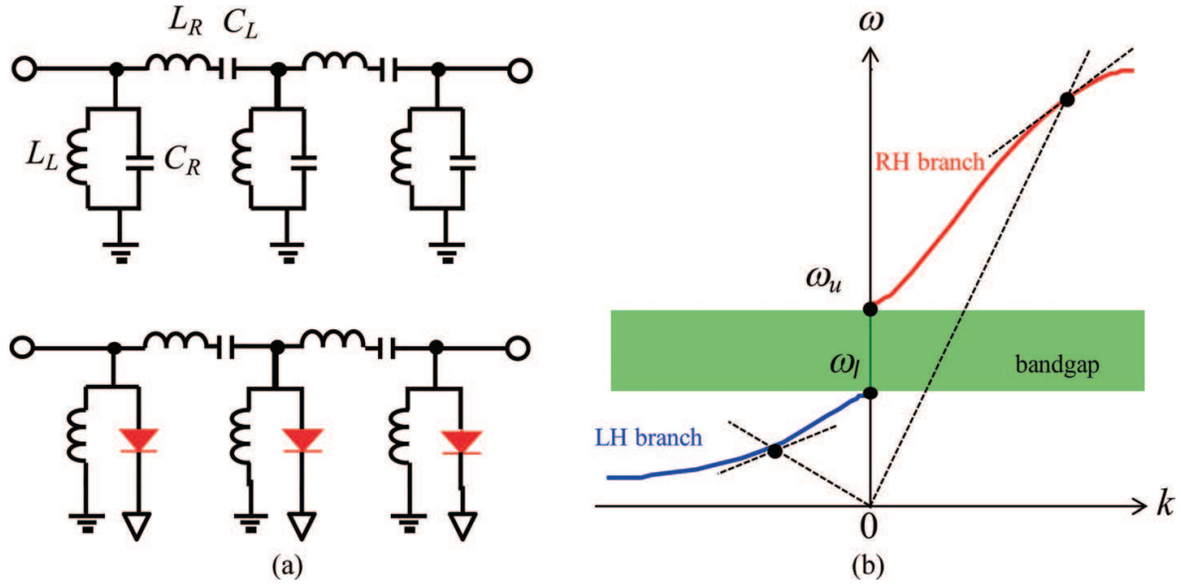

Figure 1. Structure of nonlinear CRLH lines. (a) The cell structures of linear (upper) and nonlinear (lower) CRLH lines and (b) the dispersion curve of CRLH lines.

$$\omega_{LH}(k) = \sqrt{\omega_x^2(k) - \sqrt{\omega_x^4(k) - \frac{1}{C_L C_0 L_L L_R}}}, \tag{2}$$

where $\omega_x(k)$ is defined as

$$\omega_x(k) = \sqrt{\frac{k^6}{720 C_0 L_R} - \frac{k^4}{24 C_0 L_R} + \frac{k^2}{2 C_0 L_R} + \frac{1}{2 C_0 L_L} + \frac{1}{2 C_L L_R}}. \tag{3}$$

Furthermore, $V_g(k)$ represents the group velocity of the line explicitly given by

$$V_g(k) = \frac{k\left(k^4 - 20k^2 + 120\right)}{240 C_0 L_R} \frac{\omega(k)}{\omega_x^2(k) - \omega^2(k)}, \tag{4}$$

where $\omega = \omega_{LH}(k)$ for the LH branch and $\omega = \omega_{RH}(k)$ for the RH branch. Typical behavior of $\omega(k)$ is shown in **Figure 1(b)**. There are two essential frequencies that characterize the lines' dispersive nature ω_{se} and ω_{sh} defined by $1/\sqrt{C_L L_R}$ and$1/\sqrt{C_0 L_L}$, respectively. It is found that the line exhibits a LH property at frequencies lower than $\omega_l \equiv \min(\omega_{se}, \omega_{sh})$ and an ordinary RH property at frequencies higher than $\omega_u \equiv \max(\omega_{se}, \omega_{sh})$. When $\omega_{se} = \omega_{sh}$, the LH branch is continuously connected with the RH one, and the line is called *balanced*. On the other hand, when ω_{se} is not coincident with ω_{sh}, a stop band, where all supporting modes become evanescent, appears between ω_l and ω_u, and the line is called *unbalanced*. One of the noteworthy properties of LH waves is that the wavelength becomes longer as the frequency increases at least locally. In

addition, the envelop wave (accordingly, the power) moves to the different direction from its carrier wave, because $V_g(k)$ has the opposite sign to the phase velocity.

To introduce nonlinearity, we employ the Schottky varactor in place of C_R as shown at the bottom of **Figure 1(a)**. The Schottky varactor is a special type of a diode, whose capacitance is varied by the terminal voltage that biases reversely. In general, its capacitance voltage relationship is modeled as

$$\mathrm{C}(V) = C_0\left(1+\frac{V_0}{V_J}\right)^m\left(1+\frac{V}{V_J}\right)^{-m}, \tag{5}$$

where C_0, V_J, and m are the zero-bias junction capacitance, junction potential, and grading coefficient, respectively. In addition, the cathode of the Schottky varactor is biased at V_0. Using this representation, the transmission equations are given by

$$L_R\frac{d^2I_n}{dt^2} = -\frac{I_n}{C_L} - \frac{d}{dt}(V_n - V_{n-1}), \tag{6}$$

$$C_R\frac{d^2V_n}{dt^2} = -\frac{V_n}{L_L} + \frac{d}{dt}(I_n - I_{n+1}) - \frac{dC_R}{dV}\left(\frac{dV_n}{dt}\right)^2, \tag{7}$$

where I_n and V_n are the current and voltage at the nth cell, respectively.

3. Head-on collision of LH waves

It is well known that the efficiency of resonant interactions between two waves is maximized, when the phase-matching condition: $k_2 = m_1\,k_1 + m_3\,k_3$, $\omega_2 = m_1\omega_1 + m_3\omega_3$, where $k_{1,3}$ and $\omega_{1,3}$ represent the wavenumbers and angular frequencies of interacting waves, and k_2 and ω_2 represents those of the wave generated by the interaction. Moreover, $m_{1,3}$ are integers that are specified by the order of the generated harmonics. When the incident pulses have a common carrier frequency and are traveling in opposite directions, it results in the condition $k_1 = -k_3$. Hence, the maximal second harmonic generation can be observed when $k_2 = 0$. Similarly, for the third harmonic generation, k_2 has to be close to k_1. For RH waves, the higher the frequency, the shorter the wavelength; therefore, it is impossible to satisfy this condition. On the other hand, when the carrier frequencies of the interacting waves are both set to $\omega_l/2$, any CRLH lines can generate second harmonic waves effectively via head-on collisions because the second harmonic frequency ω_l corresponds to zero wavenumber. **Figure 2** shows the head-on collision of envelop pulses whose carrier frequencies correspond to $\omega_l/2$ (=1.6 GHz). To obtain **Figure 2**, we set C_0, C_L, L_R, and L_L to 1.0 pF, 1.0 pF, 2.5 nH, and 2.5 nH, respectively, so that the line becomes balanced with $\omega_u = \omega_l = 3.2$ GHz. In **Figure 2(a)**, the dispersion curve is shown, where P_1, P_2, P_3, and P_4 represent the positions on the dispersive curve the fundamental, second, third, and fourth harmonic waves occupy, respectively. Note that the wavenumber at P_2 is equal to zero, and either P_3 or P_4 exhibits coincident wavenumber with that of P_1. **Figure 2(b)** shows the calculated waveforms, where six spatial waveforms are recorded in 60-ns increments.

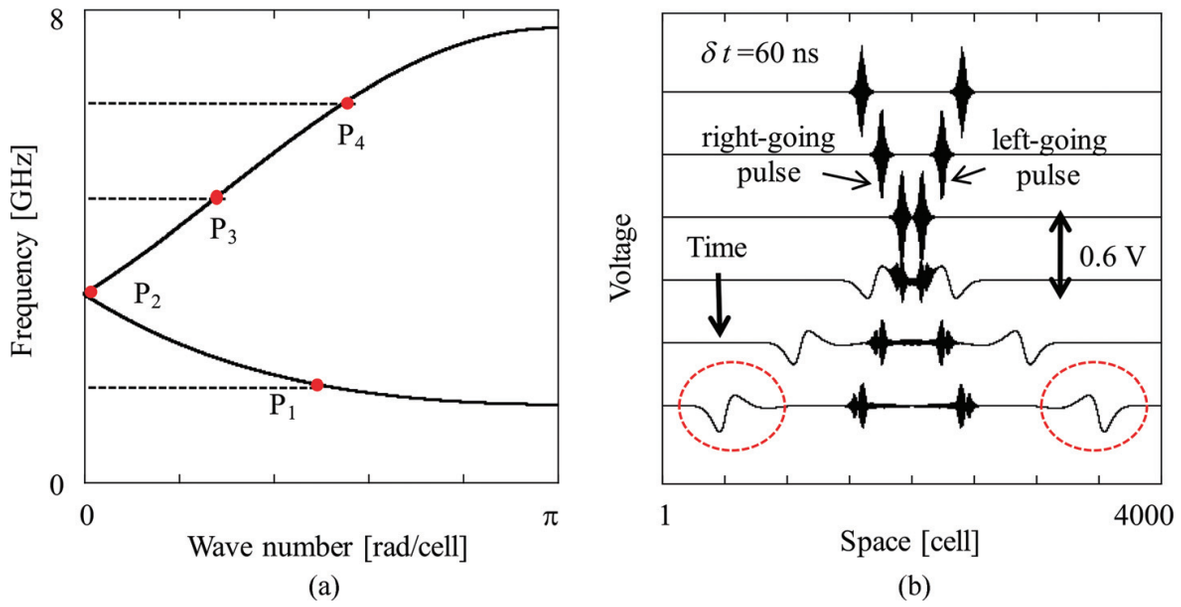

Figure 2. Second harmonic generation via head-on collision of LH waves. (a) The dispersive properties of interacting waves and (b) the numerically obtained time-domain waveforms.

Long wavelength envelope pulses result from the head-on collision as indicated by red circles. Another example is shown in **Figure 3**. The carrier frequency of the colliding pulses is set to 1.9 GHz, such that the wavenumber of the second harmonic becomes nonzero, and the wavenumber of the third harmonic becomes close to that of the fundamental wave; therefore, the resonance conditions can be satisfied for $(m_1, m_3) = (1, 2)$ and/or (2, 1). As expected, we can see that the wavelengths of the collision-induced pulses are comparable to that of the incident ones in **Figure 3(b)**. Actually, the spectral peak of the collision-induced pulses is located at

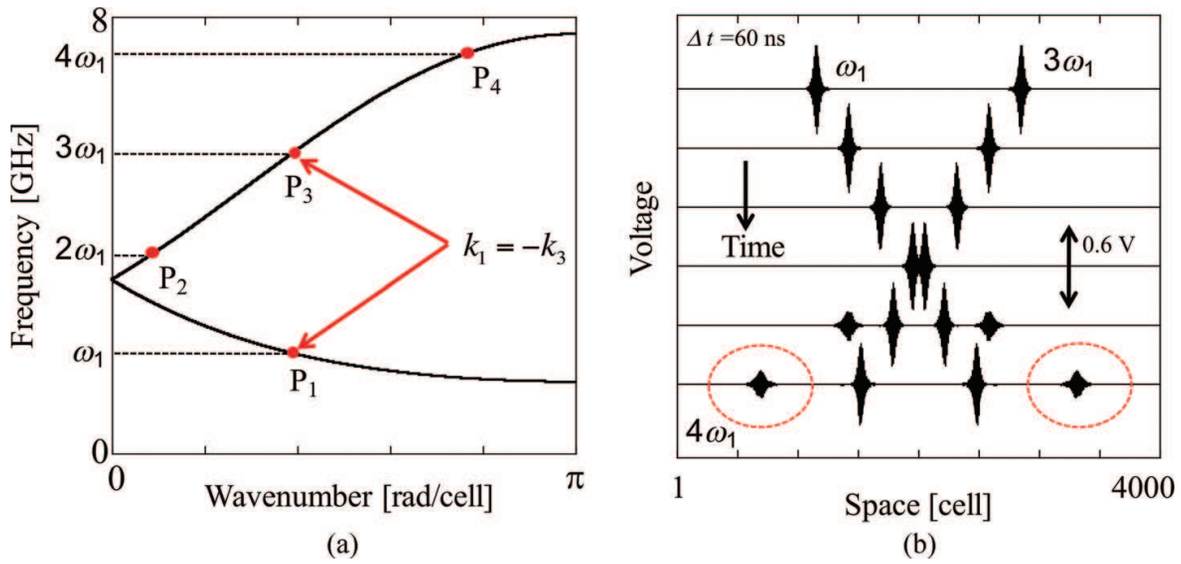

Figure 3. Fourth harmonic generation via head-on collision of LH waves. (a) The dispersive properties of interacting waves and (b) the numerically obtained time-domain waveforms.

http://dx.doi.org/10.5772/intechopen.70739

5.6 GHz, being close to the third harmonic. Note that P_3 occupies the RH branch, so that the LH waves are converted into the RH ones through resonances.

The resonance is briefly discussed for the two colliding pulses having different carrier frequencies [19]. Let the carrier frequency of the left (right)-moving pulse denote as $\omega_{1(2)}$. Then, we set ω_1 slightly higher than $\omega_l/2$, while ω_2 is fixed at $\omega_l/2$. The resulting amplitude of the wavenumber of the right-moving pulse surpasses that of the left-moving one. Both of incident pulses exhibit left-handedness; therefore, the wave vector directs to the left for the second harmonic wave. Because the second harmonic wave is carried by the RH mode, the collision-induced envelope pulse moves to the left. Similarly, only the right-moving envelope pulse develops, if ω_2 is set slightly higher than $\omega_l/2$, while ω_1 is fixed at $\omega_l/2$. These expectations were validated experimentally using bread-boarded test circuit [20].

In the next section, the evolution equations of the envelope functions of the incident and collision-induced pulses are obtained by the application of the derivative expansion method to the transmission equation of a nonlinear CRLH line [21]. In particular, the generation efficiency of the second-harmonic wave is formulated for the case when the left- and right-moving pulses have a common frequency and wavelength.

4. Three-wave mixing of LH waves

In the present study, we consider the case where the pulse spreads over many cells, and the lattice is regarded as being homogeneous, such that the discrete spatial coordinate n can be replaced by a continuous one x. Then, by series-expanding Eqs. (6) and (7), the evolution equation of the continuous counterpart of the line voltage $\psi = \psi(x, t)$ is given by

$$C_R C_L L_R L_L \frac{\partial^4 \Psi}{\partial t^4} + 4C_L L_R L_L \frac{dC_R}{dV}\frac{\partial \Psi}{\partial t}\frac{\partial^3 \Psi}{\partial t^3} + 3C_L L_R L_L \frac{dC_R}{dV}\left(\frac{\partial^2 \Psi}{\partial t^2}\right)^2 + 6C_L L_R L_L \frac{d^2 C_R}{dV^2}\left(\frac{\partial \Psi}{\partial t}\right)^2 \frac{\partial^2 \Psi}{\partial t^2} + C_L L_R L_L \frac{d^3 C_R}{dV^3}\left(\frac{\partial \Psi}{\partial t}\right)^4 + (C_L L_R + C_R L_L)\frac{\partial^2 \Psi}{\partial t^2} + \Psi - C_L L_L \frac{\partial^4}{\partial t^2 \partial x^2}\left(\Psi + \frac{1}{12}\frac{\partial^2 \Psi}{\partial x^2} + \frac{1}{360}\frac{\partial^4 \Psi}{\partial x^4}\right) = 0, \tag{8}$$

where $C_R = C(\psi - V_0)$. To quantify the resonant nonlinear processes in a nonlinear CRLH line, we apply the derivative expansion method [22] to that evolution equation. It leads to the evolution equations of envelop functions of the involved waves. We first expand the spatial and temporal derivatives as

$$\frac{\partial}{\partial x} = \frac{\partial}{\partial x_0} + \epsilon \frac{\partial}{\partial x_1} + \epsilon^2 \frac{\partial}{\partial x_2} + \cdots, \tag{9}$$

$$\frac{\partial}{\partial t} = \frac{\partial}{\partial t_0} + \epsilon \frac{\partial}{\partial t_1} + \epsilon^2 \frac{\partial}{\partial t_2} + \cdots, \tag{10}$$

for $\varepsilon << 1$. For describing the three-wave mixing process of two waves having a wave number of k_1 and k_3, then the wave number of the resulting wave k_2 satisfies the condition $k_2 = k_1 + k_3$.

As mentioned above, for efficient three-wave mixing, the frequencies must satisfy the resonant condition, that is, $\omega(k_2) = \omega(k_1) + \omega(k_3)$. The voltage variable is then assumed to have a form of

$$\Psi(x,t) = \sum_{j=1}^{3} A_j e^{i\left(\omega_j t_0 - k_j x_0\right)} + c.c., \tag{11}$$

where $\omega_j \equiv \omega(k_j)$ and A_i denotes the envelope function of variables x_1, x_2,… and t_1, t_2,… Substituting Eq. (11) into Eq. (8), the terms proportional to $e^{i(k_j x_0 - \omega_j t_0)}$ (j = 1, 2, 3) of each order of ε are collected to be vanished. From O(ε^2) terms, the evolution equations of envelope functions are governed by the 3WRI equations given by

$$\frac{\partial A_j}{\partial t} + V_g\left(k_j\right)\frac{\partial A_j}{\partial x} = G_j A_{j+1}^* A_{j+2}^*, \tag{12}$$

where j = 1, 2, 3, mod 3, and the coupling coefficients are given by

$$G_j = \frac{-i180m\omega_j C_0 L_L\left(-1 + C_L L_R \omega_j^2\right)}{\left(V_0 + V_J\right)\left\{-C_L L_L k_j^2\left(360 - 30k_j^2 + k_j^4\right) - 360C_L L_R + 360C_0 L_L\left(-1 + 2C_L L_R \omega_j^2\right)\right\}}, \tag{13}$$

whose denominator becomes zero only at $\omega_2 = (C_0 L_R C_L L_L)^{\frac{1}{4}} \in (\omega_l, \omega_u)$ so that G_2 does not exhibit any diverging behavior for frequencies in either the RH or LH branches. In particular, the head-on collision of two envelope pulses having common wavenumber, there are two cases $\omega_2 = \omega_{LH}(0)$,

$$G_2 = \begin{cases} -i\dfrac{m}{2\left(V_0 + V_J\right)}\dfrac{1}{\sqrt{C_0 L_L}}, & \omega_{se} > \omega_{sh}, \\ 0, & \omega_{se} < \omega_{sh}. \end{cases} \tag{14}$$

For $\omega_2 = \omega_{RH}(0)$

$$G_2 = \begin{cases} 0, & \omega_{se} > \omega_{sh}, \\ -i\dfrac{m}{2\left(V_0 + V_J\right)}\dfrac{1}{\sqrt{C_0 L_L}}, & \omega_{se} < \omega_{sh}. \end{cases} \tag{15}$$

In summary, the value of G_2 becomes finite only when the second harmonic frequency is matched to ω_{sh}. In contrast, for a balanced CRLH line,

$$G_2 = -i\frac{m}{4\left(V_0 + V_J\right)}\frac{1}{\sqrt{C_0 L_L}}. \tag{16}$$

Based on this G_2 property, a scheme can be proposed for converting the carrier frequency of the incident pulsed wave into its second-harmonic wave without deteriorating pulse duration. **Figure 4(a)** shows the circuit configuration of the generator creating the pulsed second harmonic waves. The nonlinear CRLH line is divided into two segments. The first and second

http://dx.doi.org/10.5772/intechopen.70739

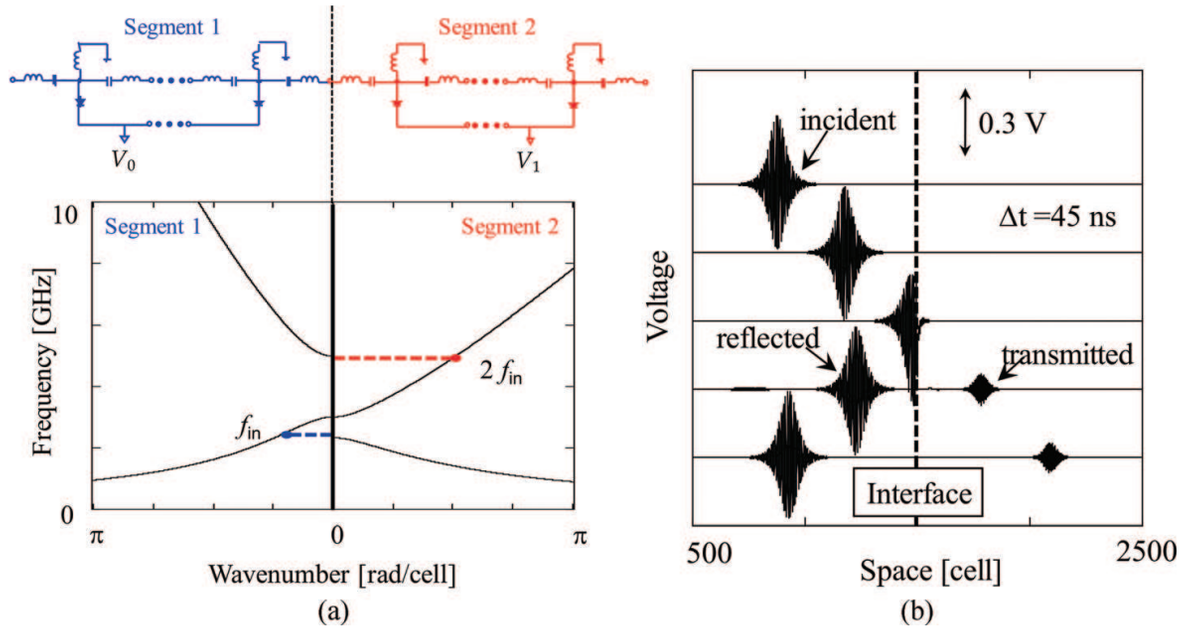

Figure 4. Effective method of second harmonic generation. (a) The device structure (upper), dispersive property of each segment (lower), and (b) the numerically obtained time-domain waveforms.

L_R (nH)	2.8	C_L (pF)	1.0	L_L (nH)	2.5
C_0 (pF)	1.0	V_J (V)	2.0	m	2.0

Table 1. Parameter values used to obtain **Figure 4**.

segments are represented by black and grey elements, respectively. The line parameter values used in the present demonstration are listed in **Table 1**. The biasing voltage to shunt varactors is the unique difference between the segments, which are labeled as V_0 and V_1 for the first and second segments, respectively. Increasing V_0 decreases the capacitance of the Schottky varactors and then increases ω_{sh}. The first segment is then arranged for V_0 to be sufficiently large to satisfy the condition $\omega_{sh} > \omega_{se}$. An envelope pulse, whose carrier frequency fin is half as high as $\omega_{sh}/2\Pi$, is then inputted to the first segment. In contrast, V_1 is set to be small in order to lower ω_{sh} such that the stop band includes f_{in}. The typical dispersion that the segments must have is shown in **Figure 4(b)**. Here, V_0 and V_1 are set to 2.7 and 0.2 V, respectively. The left- and right-side dispersion curves are for the first and second segments, respectively. The incident pulse cannot be transmitted into the second segment because f_1 is designed to be in the stop band. It is then reflected at the interface. The reflected pulse interacts with the incident pulse in the same manner as the oppositely traveling pulse. The condition $\omega_{sh} > \omega_{se}$ guarantees that G_1 becomes finite. Consequently, the second-harmonic wave develops in the first segment at the vicinity of the segments interface. Because the group velocity at $\omega_{RH}(0)$ is zero in the first segment, the second-harmonic wave remains around the interface. This stationary oscillation is partially transmitted into the second segment, resulting in the pulsed second harmonic wave

moving to the right on the second segment. The second harmonic pulse is uniquely obtained at the end of the second segment. **Figure 4(c)** shows the numerically obtained evolution of a single soliton having a carrier frequency of f_{in}. Five spatial waveforms recorded at 45 ns intervals are plotted. We can observe that the right-moving incident pulsed wave is reflected at interface *P*, and a small envelope pulse is transmitted into the second segment. The transmitted pulse has only one-fifth the amplitude of the incident pulse; however, it preserves pulse shape and successfully doubles its carrier frequency.

5. Harmonic resonance

In this section, we investigate harmonic resonance in a nonlinear CRLH line [23]. As discussed in Section 1, the harmonic resonance becomes significant when the phase velocities of the fundamental and second harmonic waves are coincident. **Figure 5(a)** shows the typical dispersion of a CRLH line, where L_R, L_L, C_L, and C_0 are set to 2.5 nH, 2.5 nH, 1.0 pF, and 0.6 pF, respectively. For convenience, we also define $\alpha \equiv C_L L_R / C_0 L_L$. Notice that the line is balanced when α = 1.0. Two points P_1 and P_2 in **Figure 5(a)** correspond to the fundamental and second harmonic waves, respectively, for significant harmonic resonance. Both points are placed on a common line passing through the origin, so that the second harmonic wave has the same phase velocity as the fundamental. With k_f and ω_f as the wave number and angular frequency of the fundamental wave, harmonic resonance becomes eminent when the second harmonic wave satisfies the two conditions $k_s = 2k_f$ and $\omega_s = 2\omega_f$, where k_s and ω_s represent the wave number and angular frequency of the second harmonic wave, respectively. The second harmonic wave must occupy the RH branch. Thus, the latter condition is more precisely written as $\omega_{RH}(2k_f) = 2\ \omega_{LH}(k_f)$. Note that both P_1 and P_2 exhibit relatively small wave numbers; the

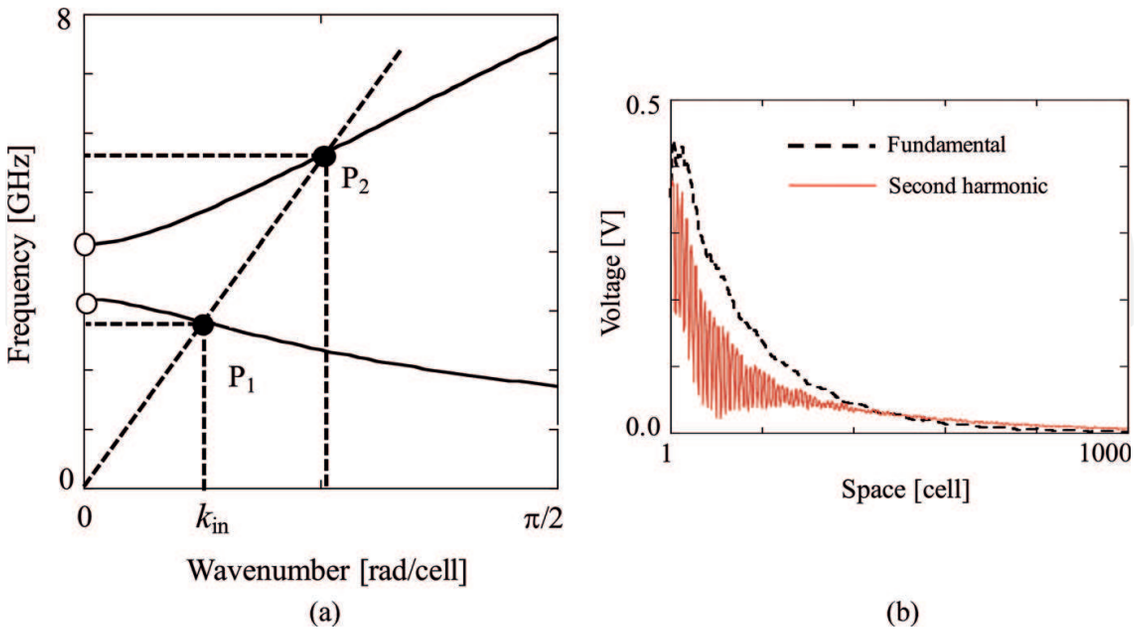

Figure 5. Harmonic resonance in nonlinear CRLH lines. (a) The operating points in dispersion curve and (b) the steady-state voltage profiles of fundamental and second harmonic waves.

second-order long-wavelength approximation suffices to describe the processes involved; therefore, the equation $\omega_{RH}(2k_f) = 2\,\omega_{LH}(k_f)$ is explicitly solved for k_f to give

$$k_f = \frac{1}{2}\sqrt{\frac{C_0}{5C_L}}\sqrt{\frac{-4\alpha^2 + 17\alpha - 4}{\alpha + 1}}, \tag{17}$$

$$\omega_f = \sqrt{\frac{5}{4C_0L_L}}\sqrt{\frac{1}{\alpha + 1}}. \tag{18}$$

Note that α must be in (1/4, 4) for the real k_f. The fundamental and second harmonic waves are then shown to have the characteristic impedance $Z_f = \sqrt{L_L/C_L}\sqrt{(4-\alpha)/(4\alpha-1)}$ and $Z_s = \sqrt{L_L/C_L}\sqrt{(4\alpha-1)/(4-\alpha)}$, respectively. Note that $Z_f = Z_s$ at $\alpha = 1.0$. According to the derivative expansion method mentioned above, the 3WRI equations that describe the fundamental and second harmonic envelope functions are described as

$$\frac{\partial A_f}{\partial t_1} + v_{gf}\frac{\partial A_f}{\partial x_1} = i\rho_f A_s A_f^* + \gamma_f A_f, \tag{19}$$

$$\frac{\partial A_s}{\partial t_1} + v_{gs}\frac{\partial A_s}{\partial x_1} = i\rho_s A_f^2 + \gamma_s A_s, \tag{20}$$

where v_{gf} and v_{gs} are the group velocities of the fundamental and second harmonic waves, respectively, explicitly given by

$$v_{gf} = -\frac{1}{\sqrt{C_0L_R}}\frac{5\sqrt{\alpha(4\alpha-1)(4-\alpha)}}{16\alpha^2 + 7\alpha + 16}, \tag{21}$$

$$v_{gs} = \frac{1}{\sqrt{C_0L_R}}\frac{5\sqrt{\alpha(4\alpha-1)(4-\alpha)}}{-\alpha^2 + 23\alpha - 1}. \tag{22}$$

Note that v_{gf} becomes negative because the fundamental wave is left-handed. The strength of harmonic resonance is determined by the coupling coefficients $\rho_{f,s}$. Because of the term A_f^2, the fundamental wave is spontaneously converted into the second harmonic. Ordinarily, the product $\rho_f\rho_s$ is negative, so that the increase of A_s results in the reduction of A_f. This negative feedback stabilizes both waves. On the other hand, the coupling coefficients are presently given by

$$\rho_f = \frac{5\sqrt{5}m}{4(V_0 + V_J)\sqrt{C_0L_L}}\frac{4-\alpha}{16\alpha^2 + 7\alpha + 16}\sqrt{\frac{1}{\alpha+1}}, \tag{23}$$

$$\rho_s = \frac{5\sqrt{5}m}{4(V_0 + V_J)\sqrt{C_0L_L}}\frac{4\alpha-1}{-\alpha^2 + 23\alpha - 1}\sqrt{\frac{1}{\alpha+1}}. \tag{24}$$

Both ρ_f and ρ_s are then shown to be positive for $\alpha \in (1/4, 4)$, such that the developing A_s enhances A_f. The second harmonic envelope wave travels backward because the phase of the

fundamental wave travels in the opposite direction to its envelope. This means that the amplitude of both the fundamental and second harmonic waves increases as the phase advances. **Figure 5(b)** demonstrates the principle of operation, where the numerically obtained steady-state profile of the voltage envelopes of the fundamental and second harmonic waves. The cell number is set to 2000. In addition, the input and output impedances are set to the characteristic impedances of the second harmonic and fundamental waves, respectively. The second harmonic wave generated by the harmonic resonance should travel to the input end. The reflection of the second harmonic wave at the input end was suppressed via the matched impedance, so the effect of the fundamental's left-handedness on the profile of the second harmonic could be seen. Small line resistors were used to suppress multiple reflections. In addition, α and λ_f were set to 1.5 and 20 cells, respectively. We applied a 0.5-V sinusoidal voltage at the left end (f_f = 1.0 GHz). Through Fourier transformation, filtering, and inverse transformation the calculated spatial voltages are separated into each wave component. The second harmonic wave was superposed in-phase and gained amplitude in the direction to the input end, as clearly shown in **Figure 5(b)**.

By setting f_0 and Z_{in} to f_f and Z_f, respectively, we achieve effective second harmonic generation. By the matched impedances, the fundamental waves can travel along the line without reflections at the ends. On the other hand, the second harmonic wave begins to travel to the input (left) end and is reflected significantly in a line that satisfies the condition $Z_s >> Z_f$. The load impedance also differs from Z_s, such that the second harmonic wave exhibits multiple reflections. Hence, the second harmonic wave becomes resonant in cavity when the cell size of the line is an integer multiple of $\lambda_f/2$, as illustrated in **Figure 6**. This cavity resonance makes the nonlinear CRLH line become an effective platform for second harmonic wave generation together with the above-mentioned positive feedback.

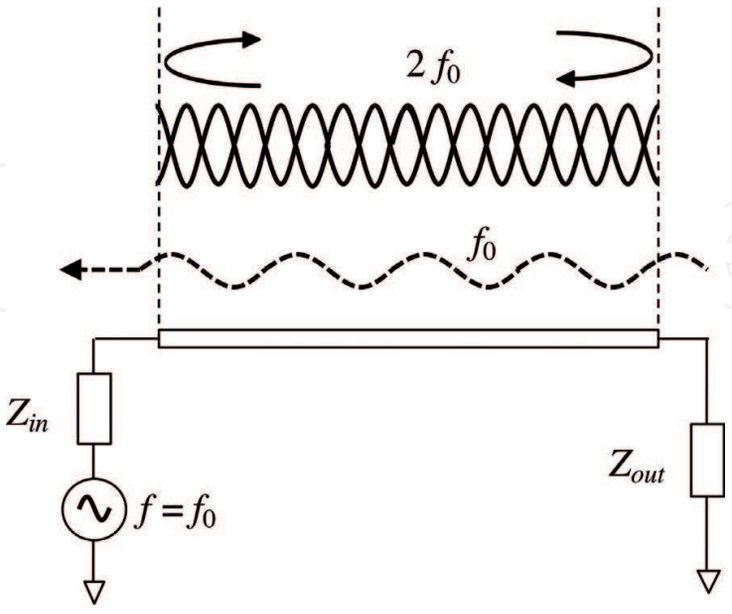

Figure 6. Practical structure for second harmonic generation using harmonic resonance.

http://dx.doi.org/10.5772/intechopen.70739

6. Soliton decay

To describe the soliton decay in a nonlinear CRLH line, we again consider the 3WRI equations of a nonlinear CRLH line. By introducing $Q_j = i\sqrt{|G_{j+1}||G_{j+2}|}A_j$, Eq. (12) is transformed into the standard 3WRI equation, that is,

$$\frac{\partial Q_j}{\partial t} + V_g(k_j)\frac{\partial Q_j}{\partial x} = \gamma_j Q_{j+1}^* Q_{j+2}^*, \tag{25}$$

where $\gamma_{1,3} = 1$ and $\gamma_2 = -1$. In what follows, an envelope having a carrier frequency of ω_j is called ω_j-envelope for brevity. When a ω_2-envelope is uniquely applied to the line and the group velocities satisfy $V_g(k_1) < V_g(k_2) < V_g(k_3)$, its evolution is predicted by solving the eigenvalue problem of the following ZS equation in the framework of the inverse scattering transform:

$$\frac{\partial u_1}{\partial x} + i\lambda u_1 = q u_2, \tag{26}$$

$$\frac{\partial u_2}{\partial x} + i\lambda u_2 = -q u_1, \tag{27}$$

where λ and $(u_1, u_2)^{\mathrm{T}}$ are the eigenvalue and corresponding eigenvector, respectively [24, 25]. In addition, $q = q(x)$ is defined by

$$\mathrm{q}(x) = -\frac{Q_2^{(0)}(x)}{\sqrt{\left(V_g(k_2) - V_g(k_1)\right)\left(V_g(k_3) - V_g(k_1)\right)}}, \tag{28}$$

for the spatial waveform $Q_2^{(0)}(x)$ of the incident ω_2-envelope. The stability of the ω_1- or ω_3-envelope solitons is shown to be secured, that is, the original envelopes never lose the solitons, while the ω_2-envelope solitons are always unstable, which decay into both the slow and fast envelope ones. The latter phenomenon is called soliton decay. When $\mathrm{Q}_2^{(0)}(x)$ evolves into N solitons, the ZS equation must have N pure imaginary eigenvalues in the upper half plane, whose norms are inversely proportional to the spatial width of the corresponding soliton. Let $\lambda_m^{(2)}(m = 1, \cdots, \mathrm{N})$ be such eigenvalues of Eqs. (26) and (27). Then, it is shown that

$$\lambda_m^{(1)} = \frac{V_g(k_3) - V_g(k_2)}{V_g(k_3) - V_g(k_1)}\lambda_m^{(2)}, \tag{29}$$

$$\lambda_m^{(3)} = \left(1 - \frac{V_g(k_3) - V_g(k_2)}{V_g(k_3) - V_g(k_1)}\right)\lambda_m^{(2)}, \tag{30}$$

where $\lambda_m^{(j)}(j = 1, 3)$ defines the eigenvalue corresponding to the soliton in the ω_j-envelope resulting from the decay of the soliton in the ω_2-envelope corresponding to $\lambda_m^{(2)}$. For example,

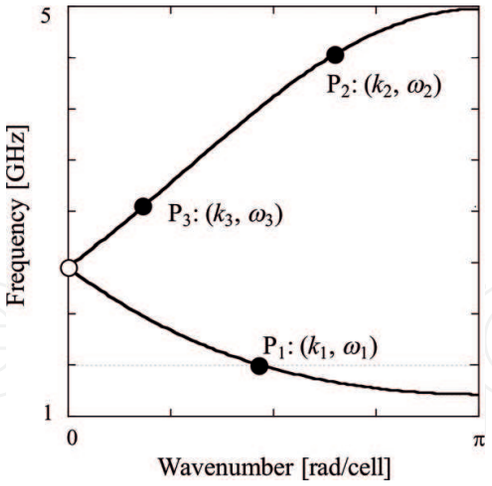

Figure 7. Dispersive properties of waves involved by soliton decay.

the line can be designed to exhibit dispersive property shown in **Figure 7**, where the incident envelope occupies the region in the neighborhood of P_2. Then, due to the resonant conditions, $\omega_{1,3}$-envelope is shown to be around $P_{1,3}$ uniquely. Notice that group velocities satisfy $V_g(k_1) < V_g(k_2) < V_g(k_3)$ and P_1 is on the LH branch. Due to the negative $V_g(k_1)$, $\lambda_m^{(1)}$ takes a small value, while $\lambda_m^{(3)}$ becomes rather large. As a result, the solitons in ω_1-envelope start to travel backward with a relatively wide width. Conversely, the ω_3-solitons become short.

We validate the analysis with the numerical integration of Eqs. (6) and (7). The line is designed to be balanced by setting C_L, L_L, C_0, and L_R to 1.0 pF, 2.5 nH, 1.69 C_L, and 1.69 L_L, respectively. In addition, m, V_J, V_0, and ω_2 are set to 2.0, 2.0 V, 1.0 V, 4.54 GHz, respectively. **Figure 8(a)**

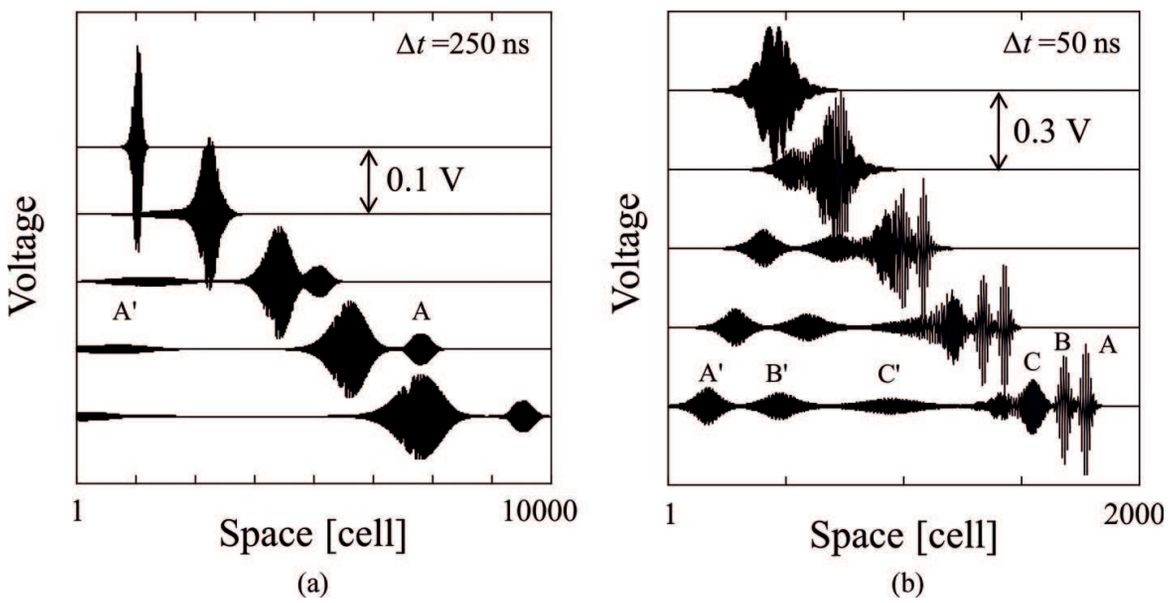

Figure 8. Numerically obtained waveforms exhibiting soliton decay. The dynamics are shown for (a) short and (b) wide envelope pulse incidences.

shows calculated waveforms on the line, where five spatial waveforms recorded at 250-ns increments are plotted. A 0.25 V hyperbolic secant envelope with 3.5-ns duration is applied at the left end. The incident ω_2-envelope decays into a unique pair of the fast and slow solitons, which are labeled at the fourth waveform as A and A', respectively. The duration of the incident ω_2-envelope is varied to be 10.5 ns in **Figure 8(b)**. Three times wider pulse is inputted for **Figure 8(b)** than one for **Figure 8(a)**. The incident ω_2-envelope decays into three pairs of the fast and slow solitons, which are labeled as (A, A′), (B, B′), and (C, C′). As expected, the widths of the emitted solitons become narrower in **Figure 8(b)** than those in **Figure 8(a)**.

As a broadband pulse generator, it suffices for a nonlinear CRLH line to succeed in the emission of the first pair of solitons. To output the short envelope pulse uniquely, we only set up a band-pass filter extracting frequencies around ω_3 in the subsequent stage [26].

7. CRLH-TWFETs

Figure 9(a) shows the structure of a CRLH-TWFET. Two coupled transmission lines are periodically loaded with FETs in such a way that one of the lines is connected to the gate and the other to the drain [15]. The gate line consists of the series inductor, series capacitor, shunt inductor, and shunt varactor, whose values are respectively denoted as L_{Rg}, C_{Lg}, L_{Lg}, and the Schottky varactor modeled by Eq. (5) is assigned to C_{gs}, which is introduced to control bifurcation property of the line via V_{SD}. The biasing voltage V_{GG} is applied to each transistor through the shunt inductance. On the other hand, L_{Rd}, C_{Ld}, L_{Ld}, and C_{ds} configure the unit cell of the drain line. The biasing voltage V_{DD} is applied to the drain of each transistor through L_{Ld}. Each inductor has finite parasitic resistances, which are denoted as R_{Rg}, R_{Rd}, R_{Lg}, and R_{Ld} for L_{Rg}, L_{Rd}, L_{Lg}, and L_{Ld}, respectively. The gate and drain lines are coupled via the gate-drain capacitor denoted as C_{gd}. Because of the couplings, there are at most two different modes for each frequency. Moreover, the lowest and second lowest frequency modes exhibit a LH property, whereas the other two modes exhibit right-handedness.

As in the case of nonlinear CRLH lines, the device can generate long wavelength harmonic wave via head-on collision of LH waves. Interestingly, such collision-induced wave evolves to a stationary pulse. **Figure 9(b)** demonstrates that, for the varactor, m and V_J are set to 1.5 and 5.0 V, respectively. We then set C_0 to the value, for which C_{gs} becomes 140 pF at $V = V_0 = V_{GG}$. The other reactance values are listed in **Table 2**. In general, the resistances tend to be proportional to the corresponding inductances. V_{SD} is set to 18.0 V to guarantee subcritical bifurcation. The cell size is 500. Both ends are excited by a sech-shaped envelope pulse whose carrier frequency is 7.7 MHz. The inset of **Figure 9(b)** shows the steady-state profile of the stationary solitary wave, which has a flattop waveform with a width of 30 cells.

In practice, the line parameter values fluctuate, such that finite disorder is introduced to the lattice dynamics, which effectively serves the Pieres-Nabarro potential to the wave dynamics. When the pulse cannot overcome the potential, it is partially reflected to become a stationary pulse via resonance. Thus, the stationary pulse is expected to develop more frequently on the line when the fluctuation increases. To examine the property of the practical line, we fabricated

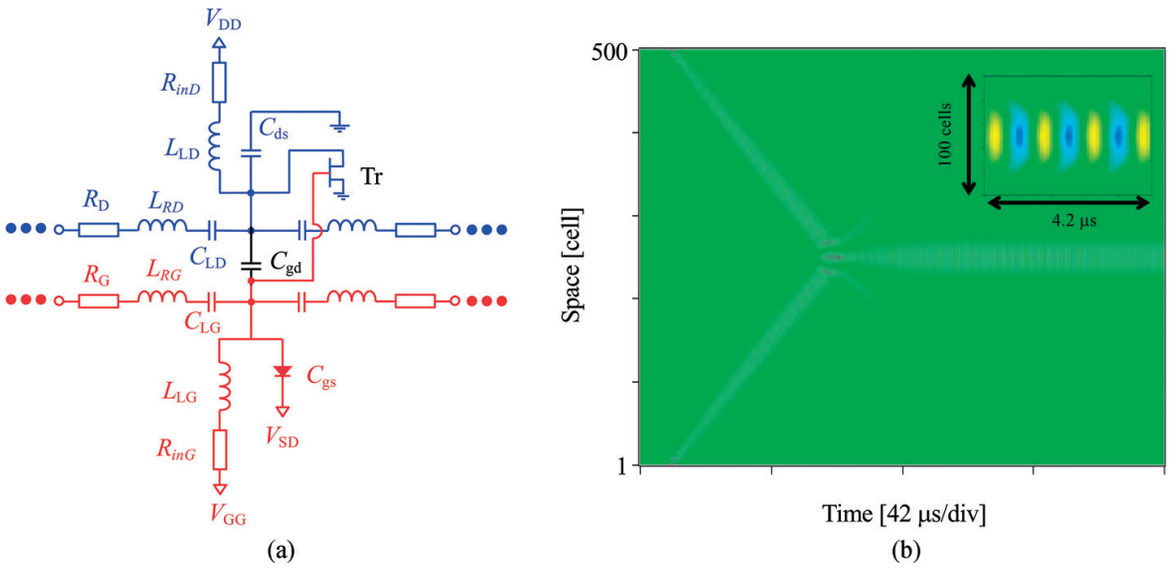

Figure 9. Head-on collision of envelop pulses in a TWFET. (a) The unit-cell structure and calculated spatiotemporal profile is shown in (b). No fluctuation of device parameter values is assumed.

C_{Lg} (pF)	22.0	C_{Ld} (pF)	22.0	L_{Lg} (μH)	10.0	L_{Ld} (μH)	4.7	L_{Rg} (μH)	4.7
L_{Rd} (μH)	10.0	R_{Lg} (Ω)	9.7	R_{Ld} (Ω)	4.5	R_{Rg} (Ω)	4.5	R_{Rd} (Ω)	9.7
C_{ds} (pF)	47.0	C_{gd} (pF)	13.0	C_{gs0} (pF)	137.0	V_J (V)	4.96	m	1.5

Table 2. Parameter values used to obtain **Figure 9(b)**.

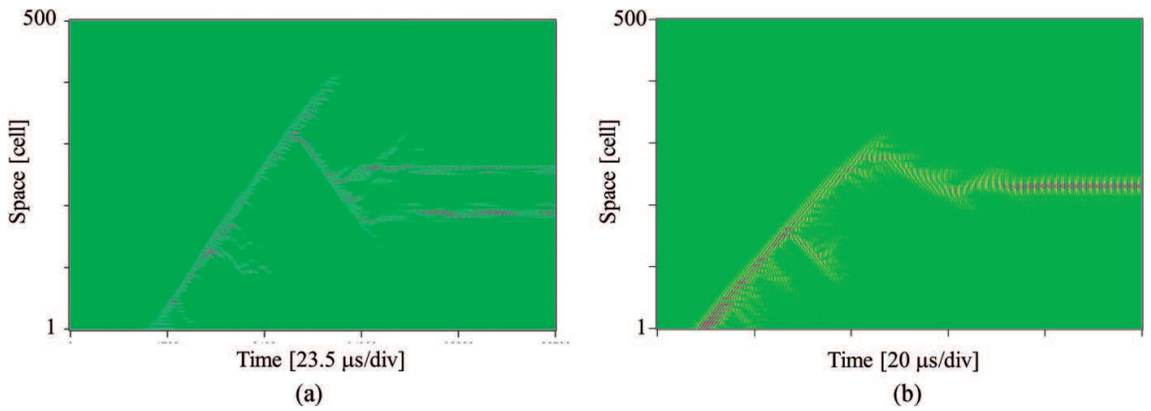

Figure 10. Envelope pulses in disordered lattice. The spatiotemporal voltage profile obtained by (a) the measurement and (b) calculation.

a test line on print circuit board. Actually, the parameter values used to obtain **Figure 9(b)** simulate those of the test line. **Figure 10(a)** shows the measured spatiotemporal voltage profile. A sech-shaped envelope pulse was inputted only at the near end. The pulse moving to the far end was significantly reflected near the 300th cell and two different stationary pulses developed after reflection. **Figure 10(b)** shows the calculated voltage profile to simulate the measured

result, where the fluctuation has 7% standard deviation. The device fluctuation cannot be modeled exactly. However, it successfully demonstrates both the reflection and the development of a stationary pulse. With the balance between the dissipation and FET gain in a disordered lattice, resonant interactions lead to this interesting wave dynamics.

8. Conclusions

We first describe the three-wave mixing process in nonlinear CRLH lines. The head-on collision of LH waves results in a significant amount of harmonic waves, whose efficiency is accurately predicted by the asymptotic method.

The CRLH dispersion allows us two spontaneous resonant processes to generate harmonic waves: the harmonic resonance and soliton decay. The harmonic resonance in a nonlinear CRLH line succeeds in generating second-harmonic waves even under the presence of finite line resistance, when the line is designed for the second-harmonic waves to cause cavity resonance. The left-handedness of the fundamental wave guarantees that both the fundamental and second harmonic waves can gain amplitude as phase advances. The soliton decay in a nonlinear CRLH line gives the effective way for generating broadband envelope pulses. The incident envelope spontaneously emits several pairs of the fast and slow solitons. In general, slow solitons exhibit left-handedness to travel backward and their fast counterparts become shorter than the incident pulse. In addition, the wider the incident pulse, the narrower the fast solitons.

A CRLH-TWFET is shown to support stationary nonlinear oscillatory pulse waves, which is generated by the collision of two counter-moving waves through resonance. The presence of disorder helps the development of stationary pulses. The bias voltage of varactor in each cell can be set independently and control the position and number of such stationary pulses.

Author details

Koichi Narahara

Address all correspondence to: narahara@ele.kanagawa-it.ac.jp

Kanagawa Institute of Technology, Atsugi, Japan

References

[1] Caloz C, Itoh T. Electromagnetic Metamaterials: Transmission Line Theory and Microwave Applications. New York: Wiley; 2006

[2] Gomez-Diaz JS, Gupta S, Alvarez-Melcon A, Caloz C. Investigation on the phenomenology of impulse-regime metamaterial transmission lines. IEEE Transactions on Antennas and Propagation. 2009;**57**:4010-4014

[3] Chi P, Itoh T. Dispersion engineering with CRLH metamaterials. In: Proceedings of IEEE International Symposium on Radio-Frequency Integration Technology. 2009. pp. 128-131

[4] Zong B-F, Wang G, Liang J, Zhang X, Wang D. Wideband frequency-scanning phased-array feed network using novel composite right/left-handed unit cell. Electronics Letters. 2016;**52**:55-57

[5] Kozyrev AB, van der Weide DW. Nonlinear wave propagation phenomena in left-handed transmission-line media. IEEE Transactions on Microwave Theory and Techniques. 2005;**53**:238–245. DOI: 10.1109/TMTT.2004.839305

[6] Simion S, Marcelli R, Bartolucci G, Sajin G, Craciunoiu F. Nonlinear composite right/left-handed transmission line for frequency doubler and short pulse generation. In: Proc. Metamaterials 2008. 2008. pp. 492-494

[7] Gupta S, Caloz C. Dark and bright solitons in left-handed nonlinear transmission line metamaterials. In: Proceedings IEEE MTT-S International Microwave Symposium. 2007. pp. 979–982

[8] Kafaratzis A, Hu Z. Envelope solitons in nonlinear left handed transmission lines. In: Proc. Metamaterials 2007. 2007. pp. 771–773.

[9] Kozyrev AB, van der Werde DW. Trains of envelope solitons in nonlinear left-handed transmission line media. Applied Physics Letters. 2007;**91**:254111–254113.

[10] Ogasawara J, Narahara K. Short envelope pulse propagation in composite right- and left-handed transmission lines with regularly spaced Schottky varactors. IEICE Electronics Express. 2009;**6**:1576-1581. DOI: 10.1587/elex.6.1576

[11] Gharakhili FG, Shahabadi M, Hakkak M. Bright and dark soliton generation in a left-handed nonlinear transmission line with series nonlinear capacitors. Progress in Electromagnetics Research. 2009;**96**:237-249. DOI: 10.2528/PIER09080106

[12] Veldes GP, Cuevas J, Kevrekidis PG, Frantzeskakis DJ. Coupled backward- and forward-propagating solitons in a composite right- and left-handed transmission line. Physical Review E. 2013;**88**:013203-013216

[13] Powell DA, Shadrivov IV, Kivshar YS. Asymmetric parametric amplification in nonlinear left-handed transmission lines. Applied Physics Letters. 2009;**94**:084105-084107

[14] Ogasawara J, Narahara K. Experimental characterization of left-handed transmission lines with regularly spaced Schottky varactors. IEICE Electronics Express. 2010;**7**:608-614

[15] Narahara K. Numerical characterization of nonlinear oscillatory waves in a composite right- and left-handed traveling-wave field-effect transistor. International Journal of Circuit Theory and Applications. 2016. DOI: 10.1002/cta.2245

[16] van Saarloos W. Fronts, pulses, sources and sinks in generalized complex Ginzburg-Landau equations. Physica D: Nonlinear Phenomena 1992;**56**:303–367.

[17] Akhmediev NN, Afanasjev VV, Soto-Crespo JM. Singularities and special soliton solutions of the cubic-quintic complex Ginzburg-Landau equation. Physical Review E. 1996; **53**:1190-1201

[18] Descalzi O, Argentina M, Tirapegui E. Stationary localized solutions in the subcritical complex Ginzburg-Landau equation. International Journal of Bifurcation and Chaos. 2002;**12**:2459-2465

[19] Narahara K. Collision of nonlinear envelope pulses developed in composite right- and left-handed transmission lines periodically loaded with Schottky varactors. Progress in Electromagnetics Research C. 2011;**21**:1-12

[20] Narahara K, Yamane Y. Experimental observation of collision of nonlinear envelope pulses in left-handed transmission lines periodically loaded with Schottky varactors. Progress in Electromagnetics Research C. 2012;**26**:59-70

[21] Narahara K. Efficiency of three-wave mixing in nonlinear composite right- and left-handed transmission lines. IEICE Electronics Express. 2014;**11**:1-8

[22] Jeffrey A, Kawahara T, editors. Asymptotic Methods in Nonlinear Wave Theory. London: Pitman; 1982

[23] Narahara K. Harmonic resonance in a composite right-handed and left-handed transmission line periodically loaded with Schottky varactors. International Journal of Circuit Theory and Applications. 2016;**44**:492-503

[24] Zakharov VE, Manakov SV. The theory of resonance interaction of wave packets in nonlinear media. Soviet Physics, JETP. 1975;**42**:842-850

[25] Kaup DJ, Reiman A, Bers A. Space-time evolution of nonlinear three-wave interactions. I. Interaction in a homogeneous medium. Reviews of Modern Physics. 1979;**51**:275-309

[26] Narahara K. Soliton decay in composite right- and left-handed transmission lines periodically loaded with Schottky varactors. IEICE Electronics Express. 2014;**11**:1-10

IntechOpen